Journal of Electrostatics 67 (2009) 672–677

Contents lists available at ScienceDirect

Journal of Electrostatics

journal homepage: www.elsevier.com/locate/elstat

Electrodeposition in highly viscous media: Experiments and simulations

S. Gutman Grinbank, G. Díaz Costanzo, A. Soba, G.A. González*, G. Marshall

Laboratorio de Sistemas Complejos, Departamento de Computación, Facultad de Ciencias Exactas y Naturales, Universidad de Buenos Aires, C1428EGA Buenos Aires, Argentina

ARTICLE INFO

Article history:
Received 10 June 2006
Received in revised form
25 January 2009
Accepted 26 January 2009
Available online 21 February 2009

Keywords:
Electrodeposition
Viscosity
Ion transport
Numerical simulations

ABSTRACT

Electrolyte viscosity plays an important role in ion transport. Here we study the effects of high viscosity variations in thin-layer electrochemical deposition (ECD) under constant-current conditions through experimental measurements and theoretical modelling. The viscosity was varied through glycerol and polymer additions and the tracking of convective fronts was performed through the use of optical and particle image velocimetry techniques with micron sized particles. The theoretical model, written in terms of dimensionless quantities, describes diffusive, migratory and convective ion transport in a fluid under constant-current conditions. Experiments reveal that as viscosity increases, convection decreases, while concentration gradients increase. These effects are more pronounced when the current increases. Theory and simulations predict that as viscosity increases, the Poisson and Reynolds numbers decrease whereas the Peclet and electric Grashof numbers increase. Therefore, electroconvection becomes more relevant.

1. Introduction

Electrochemical deposition (ECD) of ramified deposits in thin-layer cells, producing complex geometries of fractal or dendritic character [1], is a paradigmatic model for studying growth pattern formation. Issues of ECD are particularly pertinent in the case of macrowiring using bipolar electrochemistry (spatially coupled bipolar electrochemistry, SCBE [2]), in which electrodissolution and electrodeposition in an applied electric field can be exploited to create directional growth of copper deposits between copper particles that are not connected to an external circuit. In an ECD experiment, the electrolytic cell consists essentially of two glass plates sandwiching a metal salt electrolyte and two parallel electrodes of the same metal as the electrolyte cation (the cell setup is shown in Fig. 1). When an electric current or voltage difference is applied between the electrodes, metal ions are reduced producing a ramified deposit. Cell geometry, its orientation relative to gravity, electrolyte concentration, cell current and other parameters give rise to a great variety of deposit morphologies such as fractal, densely branched or dendritic. As current flows through a thin electrochemical cell, ion concentration boundary layers develop near both electrodes. At the anode, the concentration is increased above its initial level due to the transport of ions towards the electrode together with the dissolution of metal ions. At the cathode, the ion concentration is decreased as metal ions are reduced and deposited while anions drift away. These concentration variations lead to density variations, and so to the development of gravity-driven convection rolls at the electrodes. This flow was studied in [3] using a particle tracking technique to measure the convective velocity field.

During deposit growth, a complex ion transport process takes place, mainly governed by diffusion, migration and convection. Convection, in turn, is driven by coulombic forces due to local electric charges and by buoyancy forces due to concentration gradients that lead to density gradients. Indeed, convection increases complexity in thin-layer electrochemistry. Convection can be reduced by diminishing cell thickness [4], carrying out experiments in a cell with different orientations relative to gravity [3–5], or increasing electrolyte viscosity [6]. In this sense, viscosity could be a tool for understanding the different modes of transport in thin-layer ECD.

Several studies [3,7,8] have found that gravity-driven convection rolls initially grow in size as $t^{4/5}$, where t is time, while at later times the growth crosses over to a $t^{1/2}$ growth law. Viscosity, a key parameter in analyzing the influence of convection, was studied in [6,9] where it was varied by means of glycerol addition, from 0 to $3.5\nu_0$, where ν_0 is the viscosity of pure water. Experiments revealed that with increasing viscosity, convection decreased while concentration gradients, electric resistance and voltage increased; concentration and convective fronts slowed down, but their time scaling followed the same law as for solutions without glycerol,

* Corresponding author.
E-mail address: graciela@qi.fcen.uba.ar (G.A. González).

0304-3886/$ – see front matter © 2009 Elsevier B.V. All rights reserved.
doi:10.1016/j.elstat.2009.01.058

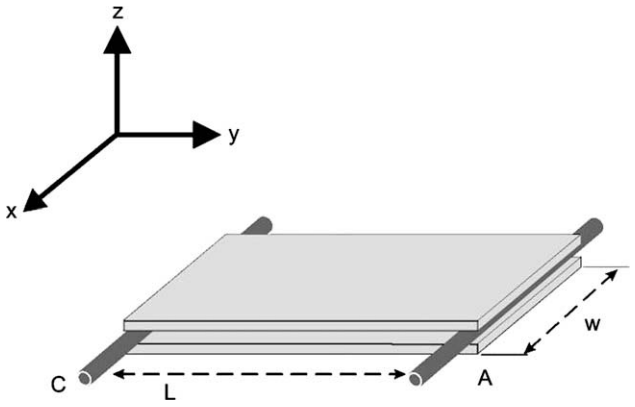

Fig. 1. Schematic diagram of the experimental cell.

only differing by a constant. In this paper, we extend those experimental results by varying viscosity in the range of 0–22.9ν_0 by adding glycerol and polyethylene oxide (PEO).

Theoretical models describing diffusive, migratory and convective ion transport in a fluid subject to an electric field under constant voltage were presented in [10–12]. In [13], a one-dimensional model for ECD under constant-current conditions was presented. Here, we extend those models to include fluid motion under constant-current conditions. The plan of the paper is to carry out simulations and then compare them with experimental measurements.

2. Experimental setup

This consists of a thin layer of unsupported electrolyte confined between two parallel glass plates (see Fig. 1). The electrolyte solution was 0.1 M $ZnSO_4$. To increase viscosity, solutions with glycerol additions of 0%, 30%, 50% and 70% in weight were employed. They correspond to viscosities of 0, 2.5, 6.05 and 22.9ν_0, respectively. Solutions with PEO additions of 1% and 5% in weight were employed as well. Zinc wire electrodes were placed at the ends of the cell with a separation of $L = 10$ mm; their thickness (0.50 mm) defined the thickness of the cell. The cell width was $w = 25$ mm. Experiments were performed under constant-current conditions. The Schlieren method was used to observe electrolyte concentration gradients [9]. For fluid tracking, latex spheres of 0.9 μm diameter were added to the fluid. A public domain software package Image [14] was used for image capturing and processing.

3. Theoretical model

Ion transport in thin-layer ECD can be described with a mathematical model based on first principles, including the Nernst–Planck equations for ion transport, Poisson's equation for the electric potential, and the Navier–Stokes equations for the fluid flow. The three-dimensional dimensionless system of equations can be written as

$$\frac{\partial C_i}{\partial t} = -\nabla\cdot\mathbf{j}_i \tag{1}$$

$$\mathbf{j}_i = -M_i C_i \nabla\phi - \frac{1}{Pe_i}\nabla C_i + C_i\mathbf{v} \tag{2}$$

$$\nabla^2\phi = Po\sum_i z_i C_i \tag{3}$$

$$\frac{\partial\boldsymbol{\zeta}}{\partial t} + \nabla\times(\boldsymbol{\zeta}\times\nu) = \frac{1}{Re}\nabla^2\boldsymbol{\zeta} + \sum_i\left[G_e z_i(\nabla\phi\times\nabla C_i) - G_{g_i}\nabla\times\left(C_i\frac{\mathbf{g}}{g}\right)\right] \tag{4}$$

$$\boldsymbol{\zeta} = -\nabla^2\Psi \tag{5}$$

$$\mathbf{v} = \nabla\times\Psi \tag{6}$$

Here C_i and $\mathbf{j}_i$ are the dimensionless concentration and flux of the ith ionic species (for a ternary electrolyte such as $ZnSO_4/H_2SO_4$, i = C, A and H, standing for zinc, sulphate and hydrogen ions); $\mathbf{v}$, ϕ, $\boldsymbol{\zeta}$ and $\boldsymbol{\Psi}$ are the dimensionless fluid velocity, electrostatic potential, vorticity vector and velocity potential vector, respectively; $\mathbf{g}/g$ is a unit vector pointing in the direction of gravity. The quantities M_i, Pe_i, Po, Re, G_e and G_{g_i} stand for the following dimensionless numbers: Migration, Peclet, Electric Poisson, Reynolds, Electric Grashof and Gravity Grashof numbers, respectively (see details in [10–12]). z_i is a signed quantity, being positive for cations and negative for anions; g is the dimensional gravitational acceleration. For system closure, a Boussinesq-like approximation has been used for the fluid density (details in [12]).

The three-dimensional model presented here is treated as a separate set of two two-dimensional models in a horizontal plane and a vertical plane, respectively [10]. The horizontal plane model constitutes the top view model while the vertical plane model constitutes the side view model (see Fig. 2). The top view model is invariant under the force of gravity (which is normal to the plane of the cell). In the side view model, electric and gravity forces are coplanar.

The boundary conditions for the velocity potential vector for both models are as follows: In a planar impermeable surface, the vector is normal to the surface and its gradient is zero; at nonslip surfaces, the tangential derivative of the velocity components is zero. The boundary and initial conditions for the top view model

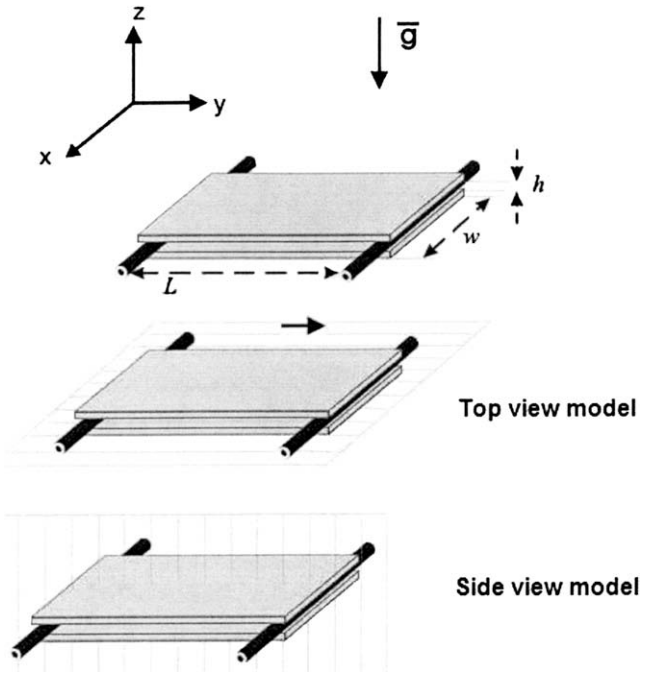

Fig. 2. Geometric definition of top and side view model. The domain of each model is defined by the intersection of the cell and the depicted plane.

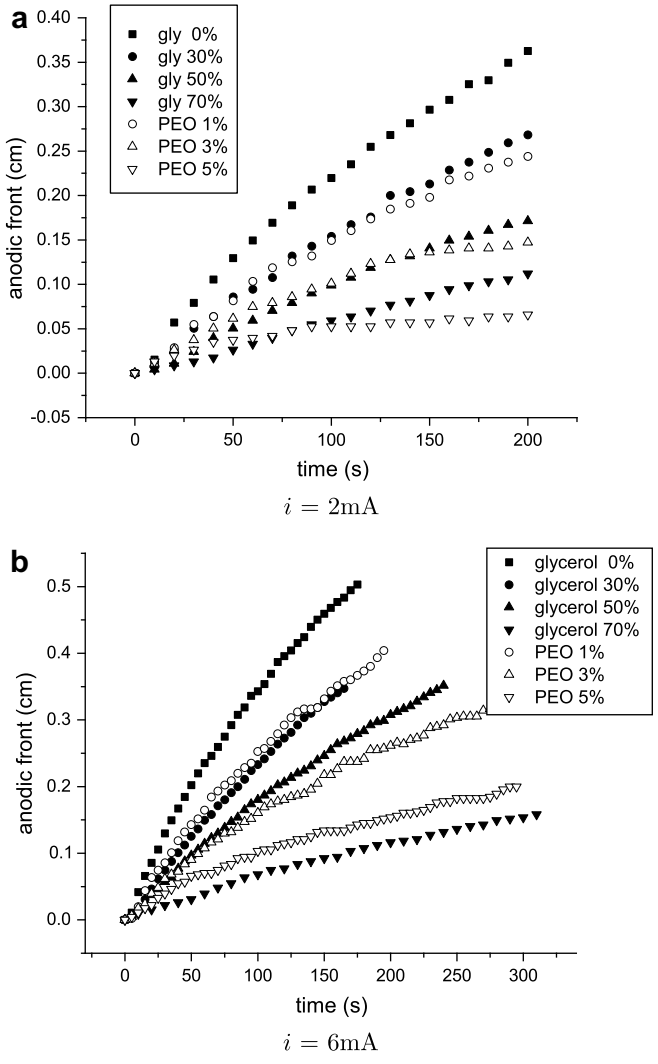

Fig. 3. Temporal evolution of the anodic front.

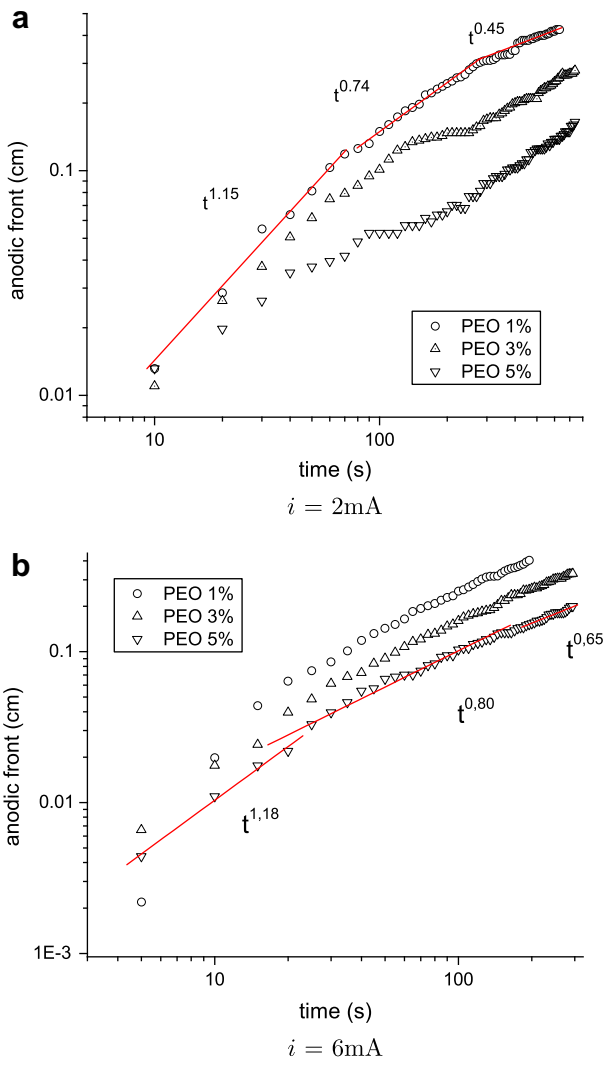

Fig. 4. Temporal evolution of the anodic front on a logarithmic scale.

(side view conditions are described in the y–z domain) under constant-current conditions in an ECD simulation [13] on the cathode and deposit are as follows:

$$\phi(x,y) = -\frac{kT}{z_C e \phi_0}\ln[z_C C(x,y)] \tag{7}$$

$$\frac{\partial C}{\partial n}(x,y) = 0 \tag{8}$$

$$J_A(x,y) = 0 \tag{9}$$

where J is the current density. For the anode, we have

$$J_C(x,y) = \frac{J}{z_C e} \tag{10}$$

$$J_A(x,y) = 0 \tag{11}$$

$$\phi(x,y) = JL(t)\iint \frac{\mathrm{d}x\,\mathrm{d}y}{\sum_i z_i C_i \mu_i} \tag{12}$$

where in Equation (12) the cell resistivity is assumed to be of migratory nature, thus neglecting diffusion effects in calculating the total voltage drop in the cell. Before defining factor $L(t)$ of Equation (12), we would like to review some concepts. In a constant-current densely branched morphology ECD experiment the main cause of the voltage drop is due to the evolution of the deposit (distance between the cathode/deposit and anode is reduced) and the cell resistance is proportional to one minus the dimensionless position of the deposit front. In addition, the distance between the deposit front and the cathodic concentration front (cation reduction and anion migration to the anode) is *almost* constant [3,13] and *short*. As our numerical model does not incorporate a growth model, we detect the position of the cathodic concentration front (instead of the deposit front) and therefore define $L(t)$ as follows:

$$L(t) = \begin{cases} 1 & \text{if } \frac{\partial C}{\partial y} = 0 \\ 1 - \min\left\{ y' \middle| y' \in [0,1], c_1 \le \frac{\partial C(y=y')}{\partial y} \le c_2 \right\} & \text{otherwise} \end{cases}$$

where c_1 and c_2 are some given positive constants. When the ion concentrations[1] are homogeneous, the first part of the function definition applies. The second part of the definition defines the y-

[1] Note that $L(t)$ is defined in terms of C. Was it defined in terms of A the result would not significantly vary.

axis position where the homogenous ion concentration at the bulk of the solution meets with the non-homogeneous ion concentration.

For the lateral sides, the boundary conditions are

$$\frac{\partial C}{\partial n} = \frac{\partial A}{\partial n} = \frac{\partial \phi}{\partial n} = 0 \tag{13}$$

At $t = 0$, ion concentrations are homogeneous, the electrostatic potential is ramp function $((\phi(t = 0))/\partial x$ is zero and $(\phi(t = 0))/\partial y$ is a constant greater than zero), and the velocity field is zero.

4. Experimental and numerical results

The addition of glycerol modifies the dielectric constant of the solution and also the cell resistivity. Fig. 3a and b shows for currents of 2 and 6 mA, respectively, the time evolution of the anodic front for different glycerol and PEO additions. We study the anodic front which is not perturbed by the deposit front. While the viscosity of the solution as a function of glycerol additions is known, this is not the case for PEO. These results reveal that gravitoconvective fronts yield a similar pattern whether for glycerol or for PEO solutions when the electric current is varied. With the goal of analyzing front evolution when viscosity is varied while the resistivity is kept constant, Fig. 4a and b shows the evolution of anodic fronts on a logarithmic scale for PEO additions alone. They reveal that initially the time scaling goes as $t^{4/5}$; at longer times we conjecture that the time scaling will tend to $t^{1/2}$. (Cell length and deposit growth do not allow the tracking of the evolution of the front for these range of values, though they present a similar behavior to previous works [6]). When viscosity is increased, the anodic front has the same behavior except for a displacement from the origin.

Fig. 4a and b shows that for low density currents (the average current densities at 2 and 6 mA are 16 and 48 mA/cm^2, respectively), the transition towards a diffusive regime ($t^{1/2}$ growth law) requires less time than for higher density currents. Although current density varies significantly during the process (area and deposit morphology are substantially modified), viscosity prevails, damping the front more rapidly.

As previously shown [6,9], at the lower range of viscosity, increasing viscosity leads to a considerable decrease in convection, and the electroconvective motion takes a longer time than the gravitoconvective motion. In addition, the damping effect of viscosity is compensated by the increment of the electric field as a consequence of higher glycerol concentration.

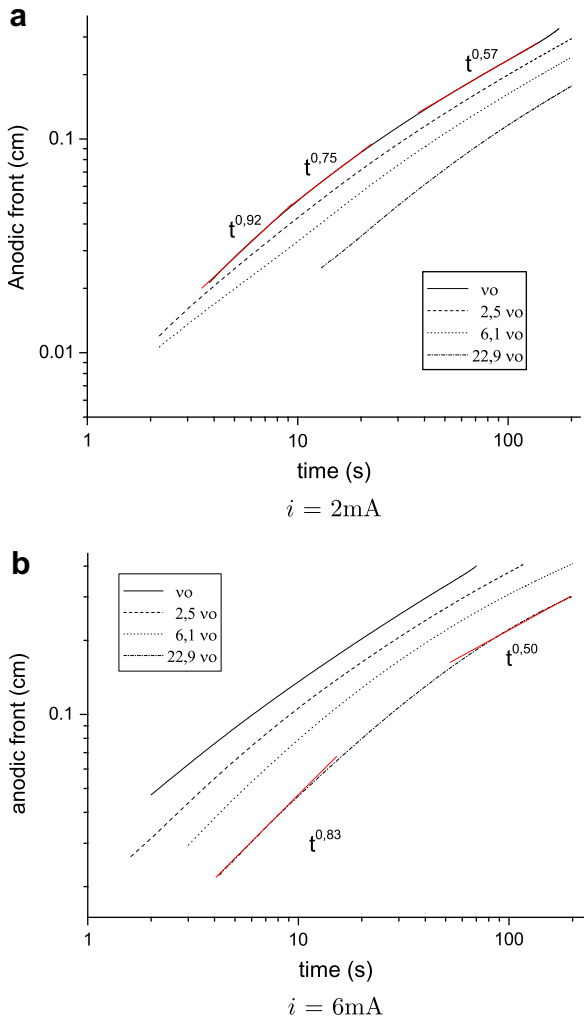

Fig. 6. Side view simulations. Temporal evolution of the anodic front on a logarithmic scale.

To analyze the dependency between electroconvection and viscosity, it is convenient to work in an experimental regime in

Fig. 5. Effect of viscosity on electroconvective motion. $i = 2$ mA.

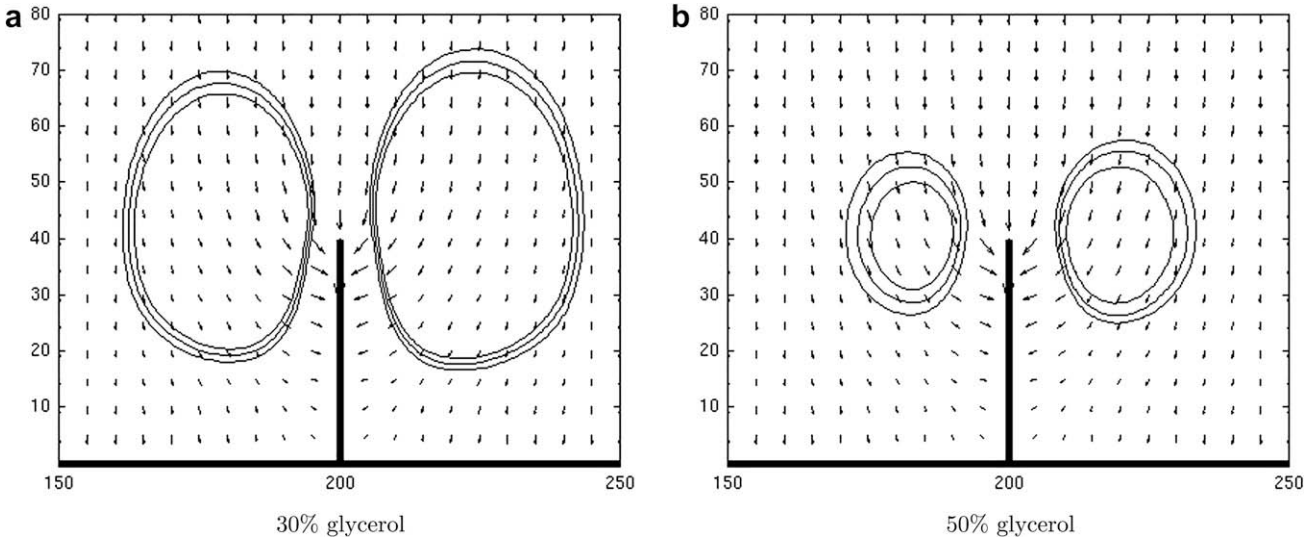

Fig. 7. Top view model simulations. Effect of viscosity on electroconvective motion. $i = 2$ mA.

which electroconvection prevails. Accordingly, we used a cell in a vertical position relative to gravity with thickness 0.1 mm and a 0.1 M $ZnSO_4$ ion concentration [15]. Fig. 5 shows the flow surrounding a flat electrode (cathode) with a small protruding spike, as well as the deposit growth for different viscosities. One can readily see the attenuation in electroconvective motion when the viscosity varies from $2.5\nu_0$ to $6.1\nu_0$. Therefore in the higher range of viscosity, the damping effect of viscosity prevails.

We next discuss our numerical simulations. The computational model solves the previous system of equations, over incremental time steps in a fixed domain, using a two-dimensional uniform lattice, the finite difference method and standard relaxation techniques (details can be found in [10,11]). The simulations are described by the set of dimensionless numbers presented above. The computational model is written in the C language and implemented on an Itanium class computer under Linux. The side view model uses a rectangular cell of 400×20 nodes for different values of the dimensionless numbers, while the top view model uses a rectangular cell of 400×200 nodes for the same set of dimensionless numbers.

The evolution of the anodic front is studied using the side view model. The concentration average is calculated in the vertical direction (z-axis) and its gradient in the horizontal direction (y-axis). Fig. 6a and b shows for 2 and 6 mA currents, respectively, the time evolution of the anodic front for different viscosities on a logarithmic scale. A comparison of the simulated and experimental results shows a remarkable agreement.

Electroconvective motion is studied using the top view model. The growth is simulated by a single spike in a flat electrode (the spike is connected and perpendicular to the cathode as shown in Fig. 7). Fig. 7a and b shows respective snapshots of the electroconvective vortex and the electric field for different viscosities. The attenuation of the motion can be clearly appreciated, when viscosity increases.

5. Discussion

Through out this paper an experimental and numerical study of high viscosity fluids in ECD was presented. By employing different experimental strategies we were able to analyze several characteristics of the processes involved in ECD over a broad viscosity range. For viscosity values where our experiments reached a limitation, we employed numerical tools to perform a deeper study of those particular scenarios.

We conclude that simulations carried out are in agreement with experimental results. Both show that the time scaling of the gravitoconvective front follows the same law as for aqueous solutions for the range of viscosities employed. Gravitoconvective fronts are steeper at higher current densities. Moreover, we showed that for large viscosity variations, the damping effects over electroconvection prevail when glycerol or PEO is added.

Acknowledgment

G.A.G. and G.M. are investigators at the National Research Council of Argentina. S.G.G., G.D.C. and A.S. are partially supported by University of Buenos Aires (UBA). This work was partially supported by grants from UBACYT X122/04 and X850/06, and ANPCyT PICTR 184.

References

[1] T. Vicsek, Fractal Growth Phenomena, World Scientific, Singapore, 1992.
[2] J.-C. Bradley, H.-M. Chen, J. Crawford, J. Eckert, K. Ernazarova, T. Kurzeja, M. Lin, M. McGee, W. Nadler, S.G. Stephens, Creating electrical contacts between metal particles using directed electrochemical growth, Nature 389 (1997) 268–271.
[3] J.M. Huth, H.L. Swinney, W.D. McCormick, A. Kuhn, F.m.c. Argoul, Role of convection in thin-layer electrodeposition, Phys. Rev. E 51 (4) (1995) 3444–3458.
[4] M. Rosso, J.N. Chazalviel, V. Fleury, E. Chassaing, Experimental-evidence for gravity-induced motion in the vicinity of ramified electrodeposits, Electrochim. Acta 39 (1994) 507.
[5] J.R. de Bruyn, Fingering instability of gravity currents in thin-layer electrochemical deposition, Phys. Rev. Lett. 74 (24) (1995) 4843–4846.
[6] G. Gonzalez, G. Marshall, F. Molina, S. Dengra, Transition from gravito- to electroconvective regimes in thin-layer electrodeposition, Phys. Rev. E 65 (5) (2002) 051607.
[7] J.-N. Chazalviel, M. Rosso, E. Chassaing, V. Fleury, A quantitative study of gravity-induced convection in two-dimensional parallel electrodeposition cells, J. Phys. Soc. Jpn. 407 (1) (1996) 61–73.
[8] S. Dengra, G. Marshall, F. Molina, Front tracking in thin-layer electrodeposition, J. Phys. Soc. Jpn. 69 (3) (2000) 963–971.
[9] G. Gonzalez, G. Marshall, F.V. Molina, S. Dengra, M. Rosso, Viscosity effects in thin-layer electrodeposition, J. Electrochem. Soc. 148 (5) (2001) C479.
[10] G. Marshall, P. Mocskos, H.L. Swinney, J.M. Huth, Buoyancy and electrically driven convection models in thin-layer electrodeposition, Phys. Rev. E 59 (2) (1999) 2157–2167.
[11] G. Marshall, P. Mocskos, Growth model for ramified electrochemical deposition in the presence of diffusion, migration, and electroconvection, Phys. Rev. E 55 (1) (1997) 549–563.

[12] G. Marshall, E. Mocskos, G. González, S. Dengra, F.V. Molina, C. Iemmi, Stable, quasi-stable and unstable physicochemical hydrodynamic flows in thin-layer cell electrodeposition, Electrochim. Acta 51 (15) (2006) 3436–3445.
[13] G. Marshall, F.V. Molina, A. Soba, Ion transport in thin cell electrodeposition: modelling three-ion electrolytes in dense branched morphology under constant voltage and current conditions, Electrochim. Acta 50 (1) (2005) 3436–3445.
[14] NIH image, available from http://rsb.info.nih.gov/nih_image/download.
[15] G. González, A. Soba, G. Marshall, F. Molina, Dense branched morphology in electrochemical deposition in a thin cell vertically oriented, Electrochim. Acta 53 (1) (2007) 133–140.